Kirigami-inspired highly stretchable nanoscale devices using multi-dimensional deformation of monolayer MoS_2

Wei Zheng, [†,§] Weicheng Huang, [#] Feng Gao, [†,§] Huihui Yang, [†,§] Mingjin Dai, [†,§] Guangbo Liu, [†] Bin Yang, [#] Jia Zhang, [†] Yong Qing Richard Fu, [¶] Xiaoshuang Chen, [†] Yunfeng Qiu, [†] Dechang Jia, [‡] Yu Zhou, [‡] PingAn Hu*[,†,‡]

[†] Key Laboratory of Micro-systems and Micro-structures Manufacturing of Ministry of Education, Harbin Institute of Technology, Harbin 150080, P. R. China.

[§] School of Materials Science and Engineering, Harbin Institute of Technology, Harbin, 150080, P. R. China

[#] Condensed Matter Science and Technology Institute and Department of Physics, Harbin Institute of Technology, Harbin 150080, China.

[¶] Faculty of Engineering & Environment, Northumbria University, Newcastle upon Tyne, NE1 8ST, UK.

[‡] Institute for Advanced Ceramics, Harbin Institute of Technology, Harbin 150001, P. R. China.

ABSTRACT: Two-dimensional (2D) layered materials, such as MoS_2, are greatly attractive for flexible devices due to their unique layered structures, novel physical and electronic properties, and high mechanical strength. However, their limited mechanical strains (<2%) can hardly meet the demands of loading conditions for most flexible and stretchable device applications. In this paper, inspired from Kirigami, ancient Japanese art of paper cutting, we design and fabricate nanoscale Kirigami architectures of 2D layered MoS_2 on a soft substrate of PDMS using a top-down fabrication process. Results show that the Kirigami structures significantly improve the reversible stretchability of flexible 2D MoS_2 electronic devices, which is increased from 0.75% to ~15%. This increase in flexibility is originated from a combination of multi-dimensional deformation capabilities from the nanoscale Kirigami architectures consisting of in-plane stretching and out-of-plane deformation. We further discover a new fundamental relationship of electrical conductance and large strain in MoS_2 Kirigami structures through both experimental work and finite element simulation. Results show that the electrical conductance of the stretchable MoS_2 Kirigami is closely related to its different stages of structural evolutions under strain: e.g., elastic stretching; then a combination of elastic stretching and out-of-plane buckling; and finally stretching and structural damage. This method provides a new opportunity to fabricate highly flexible and stretchable sensors and actuators using different types of 2D materials.

INTRODUCTION

Flexible and portable devices have become the mainstream trend in modern electronics and optoelectronics, showing wide-spread applications in in-situ health monitoring, intelligence interfaces, portable facilities for military camping, and information communication.[1-4] Realization of fully flexible electronics generally needs the devices to possess the abilities to be folded, bent, and stretched, but still maintain their original properties. Conventional electrical systems based on hard and brittle silicon and its associated technologies cannot satisfy this requirement, which pushes scientists to explore other types of highly elastic materials. In the past decade, various materials including inorganic ceramic materials, metallic materials, conductive polymer and various nanomaterials[5-11] have been exploited for fabricating different flexible devices (e.g. strain sensors and bendable display screens) to meet the requirements of both good mechanical properties and excellent electrical performances. Very recently, two-dimensional (2D) layered materials (e.g. graphene and MoS_2) have been attractive as candidates for building flexible devices, due to their atomically layered structure, layer number dependent electrical properties, super-mechanical strength (e.g. monolayer MoS_2 with a 180 ± 60 Nm^{-1}) and relatively large stretchability.[12-17] However, many current flexible devices can only withstand a limited mechanical strain, such as <1% for inorganic ceramic materials, <1% for metallic materials and <5% for conductive polymer[18] and 0.8~5% for 2D layered film of graphene and MoS_2.[19, 20] Under severe deformation conditions, this limited strain of the flexible electronics hinders their wide applications. For portable device applications, larger deformation > 5% is often needed in some specific applications such as artificial intelligence interfaces.

Recently, attempts have been made to integrate high elasticity and multi-functionality using special functionally structural designs such as Origami[25] or Kirigami architectures.[21-27] Origami and Kirigamic are both traditional Japanese craft

techniques, which enable the fabrication of 3D structures through folding, cutting or bending from 2D sheets of paper. Kirigami mainly refers to paper cutting and Origami refers more on folding of paper.

Inspired by the concept of Kirigami, 3D functional structures can be produced in a similar way to achieve a stretchability far beyond the corresponding constituents by out-of-plane deformations of materials. Specifically, some Kirigami structures have been successfully made from graphene, graphene composites and semiconducting GaAs film, respectively.[25] Several application examples based on these Kirigami structures have been demonstrated to apply into stretchable lithium ion batteries, sunlight tracking system in solar cell, soft robotics and optics.[28, 29] Compared to their planar counterparts, Kirigami structures have advantages such as enhancement of the device performance combined with a high stretchability, which is important for flexible and portable device applications. With their intrinsic super-mechanical and physical properties, 2D layered semiconductor materials such as MoS_2 are expected to be ideal building blocks for new types of functional Kirigami architectures which will show good performance in portable electronics and optoelectronics.[30-35] However, up to now, only some theoretical analysis of mechanical properties have been done on the Kirigami structures for 2D monolayer MoS_2.[22]

In this article, we perform, for the first time, the experimental investigations in Kirigami structures of 2D layered semiconductor of MoS_2. Several MoS_2 Kirigami structures were prepared using a plasma etching approach, where the soft polydimethylsiloxane (PDMS) mold was applied as both shielding mask and flexible substrate. Raman and photoluminance (PL) spectra of the MoS_2 Kirigami structures exhibited a robust shift upon a tensile loading. The MoS_2 Kirigami structures showed a large reversible strain up to 15%, far beyond MoS_2's intrinsic reversible stretchability of 0.75%. Furthermore, we revealed the relationship between the strain and electrical properties of MoS_2 Kirigami structures through experiments and finite element simulation. We further discovered a new fundamental relationship of electrical conductance and large strain in MoS_2 Kirigami structures. The MoS_2 Kirigami structure displayed three major deformation stages upon tensile loading: i.e., elastic stretching, combination of elastic stretching and out of plane buckling, and breaking stage; therefore exhibited distinct electrical conduction behavior at each stage.

EXPERIMENTAL SECTION

Growth of large-area monolayer MoS_2 films. Monolayer MoS_2 films were grown on SiO_2/Si substrate. The substrate was treated in the piranha solution at 83 °C for 30 min and washed with isopropyl alcohol, acetone, ethanol and deionized water for 10 min, respectively. Then it was treated with O_2 plasma for 5 min. The growth process was carried out in a two-zone horizontal CVD system using MoO_3 (99.9%, Aladdin) and S (99.95%, Aladdin) powders as precursors. MoO_3 powder and the substrate were placed on a quartz substrate at the high temperature zone (~670 °C). The distance between MoO_3 powder and the substrate was 3 cm. Meanwhile, the S powder was kept in an alumina boat and located at the center of low temperature zone (~250 °C), which was at the upper stream position. During the reaction, Ar gas with a flow rate of 15 sccm was used as the gas carrier. The growth process was kept for more than 30 min under the atmospheric pressure, and then the CVD furnace was naturally cooled down to room temperature.

Fabrication of 2D MoS_2 Kirigami structure on PDMS. Firstly, different types of hard templates with various microscale structures were fabricated using Si substructure with a thickness of 1 mm through photolithography and wet etching technologies. Then, the template was fumigated using perfluorooctyltrichlorosilane ($CF_3(CF_2)_5(CH_2)_2SiCl_3$) to avoid the adherence of PDMS to the template. By carefully peeling off the PDMS from the Si template in an ethyl alcohol solution, freestanding PDMS with the designed Kirigami structures was obtained. The freshly prepared PDMS was kept in a vacuum oven for 1 hour to eliminate air bubbles. After that, the PDMS was poured into the templates and heated up to 80 ^oC for 4~5 hrs. Then the PDMS with the Kirigami structures was peeled off from the Si templates in ethyl alcohol solution and dried for 30 min. Next, a large-area MoS_2 film, which was synthesized via the CVD process, was transferred onto the Kirigami-structured PDMS substrate by a polymethyl methacrylate (PMMA) assisted transfer process.[37] Then the PDMS/MoS_2 was etched using plasma from the reverse side. The smackyglam sections of MoS_2 were etched away. Then the PMMA was removed using acetone, thus the same Kirigami structure of the MoS_2 films with the underlying PDMS substrate was obtained. After that the strain sensors of PDMS/MoS_2 Kirigami structures were fabricated by patterning Ti/Au contact onto the surface of PDMS connected using copper (Cu) wire.

Finite Element Method. Commercial finite element analysis software COMSOL Multiphysics was utilized to conduct the theoretical simulation. For the simplification, a 2D PDMS Kirigami substrate model was built with physical constants selected as follows: 0.97 kg/m^3, 50 kPa and 0.49 for density, Young's module and Poisson ratio, respectively. The deformation, stress and strain distributions of Kirigami substrate were simulated under different external strains of 5%, 10%, 15% and 20%.

DFT calculation. Theoretical calculations were performed using first principles and density functional theory (DFT) in CASTEP package. The core electrons were replaced by plane wave ultra-soft pseudopotential. The generalized gradient approximation (GGA) and Perdew-Burk-Ernzerhof (PBE) methods were applied to describe the exchange and correlation effects of valance electrons. By performing a convergence test, the k-point was set as 4×4×4 and the cut-off energy was 320 eV. The model was optimized by using a GGA+PBE method and BFGS algorithm until the convergence tolerances was satisfied. The convergence tolerances were set to be 1×10^{-6} eV, 0.1 GPa, 0.05 eV/Å, 10^{-3} Å for energy, maximum stress, maximum force and maximum displacement, respectively.

Characterizations. The obtained samples were characterized using an optical microscopy (Leica DM4500P), a scanning electron microscope (SEM, Hitachi S–4200), Raman and PL spectra (LabRAM XploRA, incident power of 1 mW, excitement wavelength 532 nm). Au electrodes were fabricated using film deposition machines (ZHD−300) and a shadow mask. Electrical measurements of the device were performed using a semiconductor analyzer (Keithley 4200 SCS) combined with a home-made three-dimensional displacement platform at room temperature of ~ 20 ^oC.

RESULTS AND DISCUSSION

The synthesis process for the highly stretchable MoS_2 devices based on the Kirigami structural approach is shown in Figure 1. Large-area MoS_2 films were synthesized using a chemical vapor deposition (CVD) which has been reported in our previous papers. [36-38] The SEM and optical images of large-area MoS_2 films are shown in Figure S1 and corresponding thickness of MoS_2 is about 0.8 nm (as shown in Figure S2), which indicated the MoS_2 is monolayer. The MoS_2 films were transferred onto the different PDMS Kirigami structures which were prepared using an injection molding method (see the details in experimental section). Subsequently, various MoS_2 Kirigami structures were obtained by plasma etching the exposed MoS_2, thus MoS_2/PDMS Kirigami structures were obtained with one example shown in Figure 1b. In this way, we obtained the MoS_2 with the same Kirigami structure as the underlying PDMS substrate as shown in Figure S3e. Stretchable devices were fabricated by depositing Ti/Au contacts onto the MoS_2 Kirigami structure (see Figure 1c). Figure 1d shows the structural changes of the Kirigami structure under a uniaxial strain, providing the MoS_2 with variable deformed shapes.

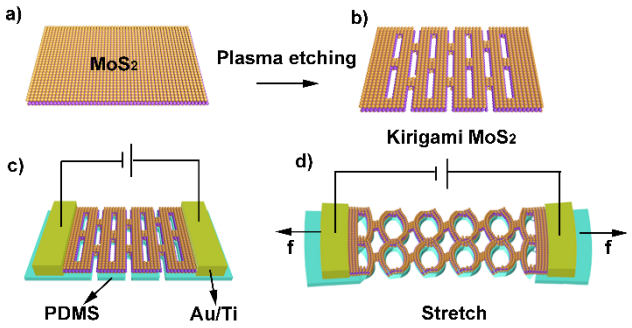

Figure 1. Schematic illustration of the fabrication process of the MoS_2/PDMS Kirigami structure.

The aforementioned technique enables the production of various MoS_2 Kirigami structures onto the PDMS substrate. The deformation behaviors between the MoS_2/PDMS and paper are similar, which makes it easy to demonstrate the Kirigami structures firstly using the paper models as shown in Figures 2a-2d. The yellow parts represent the electrodes and the white ones are the MoS_2 Kirigami structures on the PDMS substrate. As is well known, the Kirigami structure can be considered as a thin and inextensible sheet shaped into a particular 3D geometry. Here, we fabricated four different Kirigami structures: e.g., two linear patterns of Kirigami springs, Kirigami pyramids, and out-of-plane Kirigami springs with alternating C-shapes (see Figure 2). Figure 2a shows a typical Kirigami spring model with a linear pattern, and its optical and SEM images are shown in Figures $2a_1$ and $2a_2$, respectively. Each part of Kirigami spring devices is within the horizontal plane before any stain is applied; whereas an out-of-plane structural change can be generated in this Kirigami spring after a strain is applied along the *x*-axis (Figure 2b-$2b_2$). The degree of out-of-plane bending increases with increasing the deformation of the Kirigami structure. Besides the above two conventional Kirigami structures, we also prepared a Kirigami pyramid as shown in Figure 2c-$2c_2$. This Kirigami structure was able to withstand a large strain and thus allowed for popping out and out-of-plane deformation to form a pyramid shape. We also fabricated different geometric patterns of Kirigami structures with alternating C-shapes (Figure 2d-$2d_2$). This Kirigami structure enables hinge-like rotations to reduce local stress concentrations and withstands extremely large strains without fracture. These various Kirigami structures broaden the diversity of geometric construction of the MoS_2 electronic devices so that they can meet the critical demands for their wide-range applications.

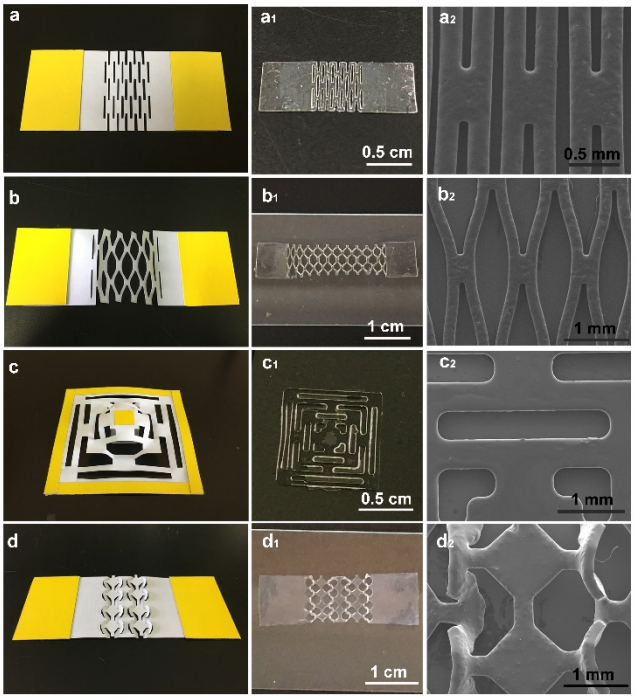

Figure 2. Different types of MoS_2/PDMS Kirigami structures. (a-d) Different types of structural models of Kirigami structures. (a_1-d_1) Optical photographs of Kirigami structures. (a_2-d_2) SEM images of MoS_2/PDMS Kirigami structures.

To study the mechanical properties and electrical device application of 2D MoS_2 Kirigami structure, the linearly patterned Kirigami spring, one of the most common Kirigami structures, was utilized as the research model. As shown in the SEM image of Figure 3a, the in-plane Kirigami spring structure undergoes a deformation by applying a strain. The elemental mapping spectrum obtained from Energy Dispersive X-ray (EDX) provides the evidence that the MoS_2 film was deposited onto the PDMS substrate (S and Mo distributions are shown in Figures 3b and 3c, respectively). Raman and PL spectra of MoS_2 Kirigami structures were investigated as a function of applied stain and the testing was carried out at the location of red point A in Figure 3a. Raman characterization was performed on both the MoS_2/PDMS and a bare PDMS with a 532 nm laser beam. The black colored curve in Figure S4 of Raman spectra is from MoS_2 on the PDMS, and red colored one is from the bare PDMS. The two peaks of E_{2g} and A_{1g} Raman modes of MoS_2 are clearly observed from Figure S4. From literature[12], the frequency difference between the E_{2g} and A_{1g} Raman modes of the 2D MoS_2 is strongly dependent on its thickness, which can be utilized for determining the layer number of MoS_2. The A_{1g} mode (out of plane mode) at 405.4 cm^{-1} and the E_{2g} mode (in plane mode) at 384.6 cm^{-1} are observed with a frequency difference of ~21 cm^{-1} (see Figure 3d), indicating that it is a monolayer of MoS_2.[12, 37]

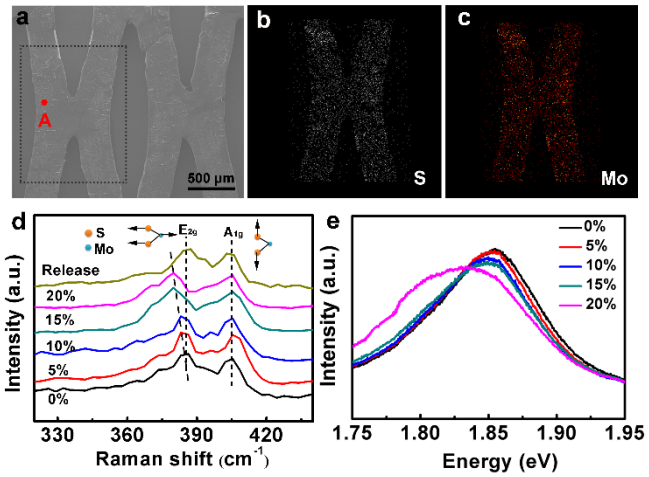

Figure 3. Characterization of structure. (a) SEM images of MoS_2/PDMS Kirigami structure under a tension. (b, c) EDX Element mapping images. (d) Raman spectra of MoS_2/PDMS composite structures under different deformation rates. (e) PL spectrum of MoS_2/PDMS composite structure under different deformation rates.

When a uniaxial tensile stress was applied to the MoS_2 crystal structure, the crystal would be elongated and the lattice spacing was increased along the uniaxial direction. This structural change can be characterized using Raman and PL spectra. Figure 3d shows Raman spectra of E_{2g} and A_{1g} modes of monolayer MoS_2 on the PDMS as a function of the uniaxial strain. The dash lines in Figure 3d label the peak centers. The frequencies of A_{1g} mode keep unchanged upon the strain applied, whereas those of E_{2g} mode exhibit an apparent blue-shift with the increase of strain. From the inset of Figure 3d, the A_{1g} mode is generated from the out-of-plane vibration of S atoms in the opposite directions, and the E_{2g} mode is resulted from the opposite vibration of two S atoms with respect to the Mo atom in the horizontal plane. The dominant covalent bonds between Mo and S atoms are sensitive to the in-plane uniaxial strain.[12] This can be utilized to verify the structural changes of monolayer MoS_2 in the Kirigami structure. The structural change of MoS_2 can also influence its PL spectra, and the corresponding results are shown in Figure 3e under different tensile strains. The PL of MoS_2 on PDMS shows a peak at around 1.86 eV, which is attributed to the lowest-energy excitation transition. This strong PL peak indicates a monolayer MoS_2 with a direct bandgap[12]. When a uniaxial strain is applied, MoS_2 Kirigami structure has a red-shift of its PL peak. Furthermore, this red-shift increases with the increase of the deformation degree: e.g., from 1.86 eV (0%) to 1.854 eV (5%), 1.849eV (10%), 1.845 eV (15%) and 1.83 eV (20%).

Electrical properties and structural differences under different strains. The influences of the strain and structural differences on the electrical properties of 2D MoS_2 Kirigami structure were further investigated. The 2D MoS_2 Kirigami structure shows a reversible stretchability up to 15% (see Figure 4a), a 20-fold increase compared to that of the conventional CVD MoS_2 (0.75% reversible stretchability as shown in Figure S6a). The electrical conductivity changed of the MoS_2 Kirigami structure show three different stages upon applying the tensile stress: e.g., an initial elastic stretching; then a combination of elastic stretching with out of plane buckling; and finally a breaking stage (see Figure 4a).

In the first stage, the deformation of MoS_2 Kirigami is within a strain value of 5%. The corresponding electrical curve of conductance (I) versus stain (ε) shows a strongly linear dependence with a slope of 0.38 (see Figure 4b). In this stage, deformation of the MoS_2 Kirigami structure mainly occurs via an elastic stretching without apparent flipping or rotation of the MoS_2/ PDMS as illustrated in Figure 4e. At this stage, the structure of monolayer MoS_2 on the PDMS surface shows a little deformation at the border or joint of the Kirigami structure (see Figures 4e and 4h), Therefore, the changes of the currents are very small with the increase of the strain during this stage as shown in Figures 4b and 4e as well as the SEM image in Figure 4h.

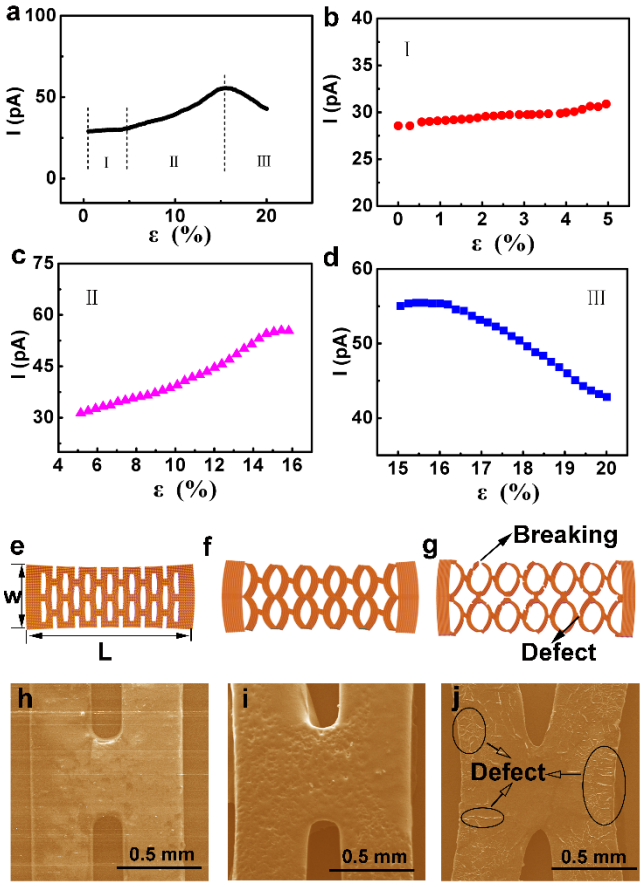

Figure 4. Relationship between deformation and electrical properties of the Kirigami devices. (a) The current-deformation curve characteristic curves based on the conventional structure and Kirigami structure devices under different deformation rates. (b-d) The electrical properties of Kirigami structure devices under different deformation rates. (e-g) Corresponding linear Kirigami structure model under different deformation rates, (e) deformation < 5%. (f) The deformation < 15%, (g) the deformation > 15%. (h-j) SEM image of Kirigami structures under different deformation rates (h) deformation < 5% (i) The deformation < 15% (j) The deformation > 15%.

In the second stage, with a strain in a range from 5% to 15%, the corresponding curve of electrical current (I) versus stain (ε) has a slope of 2.21. The conductance significantly increases upon deformation and reaches the maximum value at a deformation strain of ~ 15% (which is marked as II in Figure 4c). The Kirigami structure at the stage II exhibits out-of-plane deflections to undergo additional tensile deformation with a stain range from 5% to 15% (Figure 4f). Furthermore, the out-of-plane deformation causes a tilting angle with the horizontal plane as shown in Figure S7b. The deformation of MoS_2 at the stage II is much larger than that at the stage I,

consisting of the combination of stretching and out-of-plane buckling.

Further increase of deformation above 15% reaches the stage Ⅲ (see Figure 4a and 4d), during which the current decreases gradually as the stain is increased (see Figure 4d). With a large stain (> ~15%), MoS_2 films begin to break at the edges or joint places as shown in Figures 4g and 4j. The occurrence of breaking is usually defined as the yield point. This structural damage is irreversible. It's worth noted that the MoS_2/PDMS device with the Kirigami structure reaches the maximum reversible deformation of ~ 15%, much higher than that of the original planar MoS_2 devices with a reversible strain of only ~ 0.75 %.

To further understand the mechanical and electrical behaviors of the MoS_2 Kirigami upon tensile loading, theoretical simulation was performed on the linear Kirigami pattern using the finite element method (FEM). The generated forces from the linear Kirigami pattern were analyzed using a beam theory based on the method from literature.[29] As designed, such a sample with the linear Kirigami pattern will be bent out of plane into an angle θ with the horizontal plane under a uniaxial strain. The theoretically calculated values of θ at different strains of 5%, 10%, 15% and 20% are 17.5°, 24.5°, 29.5° and 33.5°, respectively. More information about the calculation results is shown in supporting information of Figure S7. With the increase of strain, the bent angle is increased, indicating that the PDMS substrate will be bent with a larger radius of curvature, and simultaneously the MoS_2 on the surface of PDMS will experience a larger deformation. In order to understand the distribution of stress on sample surface, FEM analysis of the linearly patterned Kirigami structure was performed, and the results are shown in Figure 5. When the strain was applied along x-axis, the structure was bent out-of-plane, resulting in locally buckling patterns. We choose a small area of Kirigami structure for analysis as shown in the red-colored square in Figure 5a. This part of the structure will be deformed according to the beam bending theory,[39] and the equations after bending deformation (Figure S8a) can be described using the following equation:

$$y = \frac{q}{24EI}(l^3x - 2lx^3 + x^4) \tag{1}$$

Any point of the bent curve can be described using the following equations:

$$\tan\gamma = \frac{\Delta y}{\Delta x} = \frac{q}{24EI}(l^3 - 6lx^2 + 4x^3) \tag{2}$$

$$\Delta x \approx \Delta l \cos\gamma \tag{3}$$

$$\varepsilon_{MoS2} = \frac{\Delta l - \Delta x}{\Delta x} = \frac{1}{\cos\gamma} - 1 \tag{4}$$

Where q is the force applied on the beam, E and I are the Young's modulus and rotational inertia, tanγ is the slope of the flexural beam equation in a position x, ε_{MoS2} is defined as the strain of MoS_2. The length of the hypotenuse was used to estimate the change of arc length Δl. The function images of tanγ within the scope of (0, l) are shown in Figure S8b. In the scope of (0, 0.5l), the values of tanγ show a decreasing function with x, which means that with the increase of x, γ decreases. At the meantime, ε_{MoS2} increases with the increase of x, which means that the maximum and minimum deformation values occur at the flexural beam center and edge, respectively.

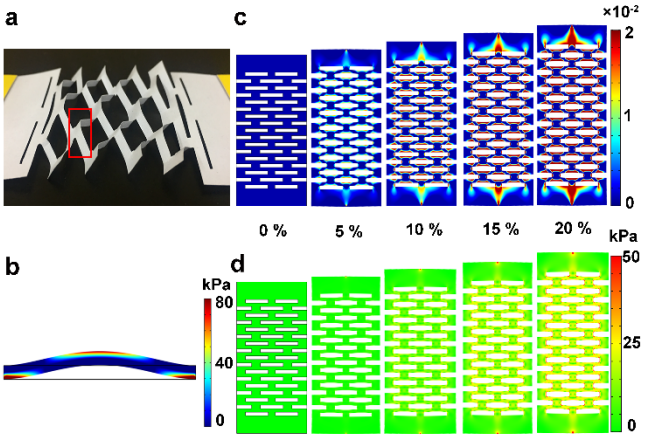

Figure 5. FEM simulation of stress distribution at different strains. (a) The model of a typical linear Kirigami structure. (b) The strain distribution of the curve beam. (c) The strain distribution of Kirigami structure under different deformation rates. (d) The stress distribution of Kirigami structure under different deformation rates.

The simulated strain distribution is shown in Figure 5b. Tensile stress concentration and associated distortions exist in the deformation processes of the Kirigami structure, which leads to the non-uniform surface stress and deformation. In our MoS_2/PDMS Kirigami experiments, one end of the Kirigami structure was fixed and the other end was stretched. The obtained displacements of the Kirigami structure under different values of deformation are shown in Figure S9. Figures 5c and 5d show the strain and stress distributions of the MoS_2 Kirigami structure under different deformations. For the Kirigami structure, the initial elastic stage is similar to the deformation of the conventional MoS_2 films (ε<5%), indicating that the deformation is mainly caused by in-plane stretching. During this stage, the strain and stress are concentrated at the connection nodes of the MoS_2 Kirigami structure. When the applied strain exceeds the critical value of ~5%, the planar deformation of the Kirigami structure will become unstable and start to be bent out of plane. At this stage, the stress can be diverted into the bending and torsional modes. With the further increase of the strain, the area of tensile stress concentration increases which means that the ε_{MoS2} value on the surface of PDMS increases. Finally, when the deformation of Kirigami structure exceeds ~15%, it will lead to the fracture of the MoS_2 films at the edge as shown in the SEM image of Figure 4j.

Practical application of the Kirigami structure devices. To verify whether the designed devices meet the stringent requirements of wearable intelligent systems and wearable healthcare applications, we fabricated a strain sensor based on the Kirigami structure. Figures 6a and 6b show the pictures of the MoS_2/PDMS Kirigami structure strain sensors applied in different situations of large deformations, for examples, on a curved surface, on the joint surfaces of a robot, or on other types of complicated surfaces. The current-voltage (I-V) characteristics of an individual Kirigami MoS_2 sensor were measured under different tensile strains. The current values were changed linearly with the voltage when different strains of 5%, 10% and 15% were applied as shown in Figure 6c.

To evaluate the potential of the proposed strain sensor for a large deformation for human-motion detection, we attached the sensor onto the knee joint of a robot as illustrated in Figure 6d. For each bending-stretching motion of the knee joint, the strain sensor reliably produced rapid, stable, and repeatable

responses. The responses of the currents were increased with the increase of deformation strain if the deformation strain value was less than 15%. The gauge factor, a performance parameter representing the sensitivity of a strain sensor, can be derived from the relation of $\Delta I/(I_\varepsilon)$. The calculated gauge factor for our sensor is about 3.5 for the applied strain of 15%. This value of the gauge factor is comparable to that of graphene fiber strain sensors.[3] The response time of the Kirigami structure-based sensor is a critical parameter. It can be seen from the time-dependent response of devices and corresponding local magnification curves in Figure S10, the response time is ~1s. To evaluate the mechanical stability of strain sensor, we apply multiple cycles under different strain as shown in Figure S11. A stable response across the cycles is observed, indicating mechanical robustness and good stability of our strain sensors. Therefore, these results showed clearly that the devices are attractive candidates for large-deformation wearable and human−machine interface applications.

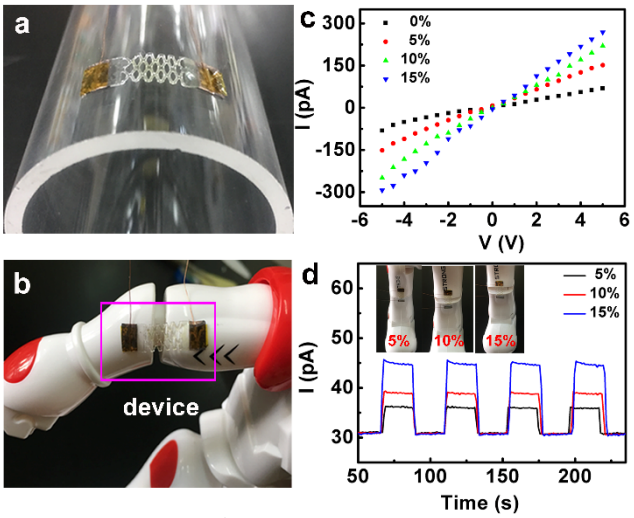

Figure 6. Applications of Kirigami structure devices. (a) The Kirigami structure devices on a curved surface. (b) The Kirigami structure devices on the surface of elbow of a robot. (c) The drain–source (*I*–*V*) characteristic curves of the devices under different deformation rates. (d) Strain sensor based on the Kirigami structure devices and the time-dependent response of devices. Inset is the photographs of knee joint of robot bending test during the measurements.

The deformation of MoS_2 Kirigami structures has a significant influence on its electrical properties. Results showed that the electrical properties of Kirigami structure devices increase slightly when the strain is below 5%, and then increase significantly in the strain range of 5~15%. After reaching the maximum value of the conductivity with the increase of applied strain up to 15%, the electrical conductivity will decrease with the further increase in the strain up to 15~20%. This unique phenomenon can be explained based on the structural changes and piezoresistive effect of the MoS_2 Kirigami structure during the deformation.

According to the theory of semiconductor physics, when the crystal is strained or compressed along one direction, the resistivity and bandgap structure of the materials will change. When applied with a uniaxial tensile stress on the MoS_2 crystal structure, the crystal will be elongated and the lattice spacing is increased along the uniaxial direction. The width of the forbidden band decreases and meanwhile the conductivity increases with the increase of tensile stress. At the meantime, the changes of bandgap structures can also affect the electrical properties. According to the literature,[40] with small strains (i. e. < 0.7%) applied, the bandgap was changed linearly with strain, thus the conductivity can be written as:

$$\sigma_{\mathrm{def}} = \sigma_{\mathrm{rel}} exp\left[-\frac{\varepsilon_{MoS_2}}{2k_BT}\frac{\partial E_g}{\partial \varepsilon}\right] \quad (5)$$

Where σ_{def} is the conductance of the film in the deformed state, and σ_{rel} is the conductance of the membrane in the relaxed state, ε_{MoS2} is the strain applied to MoS_2, and $\partial E_g/\partial \varepsilon$ is the change rate of bandgap with the strain.

Here first principle calculation work based on the density function theory (DFT) was performed to investigate how the external stress affects its band structure. The calculation results are shown in Figure S12. The band gap becomes narrowed and more tortuous band structures are generated under the applied stress (with a value around 1 GPa), which means that the value of $\partial E_g/\partial \varepsilon$ is negative and the effective masses of carriers (hole and electron) are decreased. These changes will enhance the conductance of the structure with an increase of ε_{MoS2}, therefore, the electrical conductivity of the flexible devices is increased at the beginning of the deformation. However, when the deformation strain exceeds a critical value, the MoS_2 structure will be destroyed, which can be well verified from the SEM images at different deformation states with one example shown in Figure 4j. From the image, when the deformation strain reaches ~20%, the surface of the MoS_2 films showed a lot of cracks which indicates that the MoS_2 has been fractured. Therefore, it is concluded that the suitable deformation strain of our proposed Kirigami structure devices should be less than 15%.

CONCLUSION

We successfully demonstrate a flexible device made of the 2D MoS_2 film which can achieve a significant enhancement in the electrical properties and deformation behavior by adopting the Kirigami architectures. Measurement results of electrical properties indicated that the Kirigami structures significantly improved the reversible stretchability of flexible MoS_2 electronic devices, which was increased from 0.75% to ~15%. This new design methodology bridges the gap between nanoscale and macroscale strain engineering, and enables many novel engineering applications in which a large-scale out-of-plane deflection can be controlled precisely to create multiscale and reconfigurable structures, thus will find significant applications in a variety of flexible-electronic technologies.

ASSOCIATED CONTENT

Supporting Information. This material is available free of charge via the Internet at http://pubs.acs.org.
Additional data for characterization and calculation of kirigami structure (SEM and AFM images of MoS_2 films, Optical images of preparation process, electrical properties, calculation and simulation, response and stability testing of strain sensor).

AUTHOR INFORMATION

Corresponding Author

*E-mail: hupa@hit.edu.cn.

ORCID

Wei Zheng: 0000-0001-6814-3751

Weicheng Huang: 0000-0003-3466-5169

Mingjin Dai: 0000-0001-6009-1715

PingAn Hu: 0000-0003-3499-2733

Author Contributions

W.Z and W. H. contributed equally to this work. All authors have given approval to the final version of the manuscript.

Notes

The authors declare no competing financial interest.

ACKNOWLEDGMENT

This work is supported by National Natural Science Foundation of China (NSFC, 61390502), Project supported by the Foundation for Innovative Research Groups of the National Natural Science Foundation of China (Grant No.51521003), Self-Planned Task (no. SKLRS201607B) of State Key Laboratory of Robotics and System (HIT), UK Engineering Physics and Science Research Council (EPSRC EP/P018998/1) and Newton Mobility Grant (IE161019) through Royal Society and NFSC.

REFERENCES

(1) Tian, B. Z.; Cohen-Karni, T.; Qing, Q.; Duan, X. J.; Xie, P.; Lieber, C. M., Three-Dimensional, Flexible Nanoscale Field-Effect Transistors as Localized Bioprobes. *Science* **2010**, 329, 830-834.

(2) Sekitani, T.; Zschieschang, U.; Klauk, H.; Someya, T., Flexible organic transistors and circuits with extreme bending stability. *Nat. Mater*. **2010**, 9, 1015-1022.

(3) Wang, X. N.; Qiu, Y. F.; Cao, W. W.; Hu, P. A., Highly Stretchable and Conductive Core-Sheath Chemical Vapor Deposition Graphene Fibers and Their Applications in Safe Strain Sensors. *Chem. Mater.* **2015**, 27, 6969-6975.

(4) Hu, P. A; Wang, L. F.; Yoon, M.; Zhang, J.; Feng, W.; Wang, X. N; Wen, Z. Z; Idrobo, J. C.; Miyamoto, Y.; Geohegan, D. B.; Xiao, K., Highly Responsive Ultrathin GaS Nanosheet Photodetectors on Rigid and Flexible Substrates. *Nano Lett.* **2013**, 13, 1649-1654.

(5) Yamada, T.; Hayamizu, Y.; Yamamoto, Y.; Yomogida, Y.; Izadi-Najafabadi, A.; Futaba, D. N.; Hata, K., A stretchable carbon nanotube strain sensor for human-motion detection. *Nat. Nanotechnol.* **2011**, 6, 296-301.

(6) Pang, C.; Lee, G. Y.; Kim, T. I.; Kim, S. M.; Kim, H. N.; Ahn, S. H.; Suh, K. Y., A flexible and highly sensitive strain-gauge sensor using reversible interlocking of nanofibres. *Nat. Mater.* **2012**, 11, 795-801.

(7) Liu, X. H.; Ma, T. T.; Pinna, N.; Zhang, J., Two-Dimensional Nanostructured Materials for Gas Sensing. *Adv. Funct. Mater.* **2017**, 27, 1702168.

(8) Park, M.; Im, J.; Shin, M.; Min, Y.; Park, J.; Cho, H.; Park, S.; Shim, M. B.; Jeon, S.; Chung, D. Y.; Bae, J.; Park, J.; Jeong, U.; Kim, K., Highly stretchable electric circuits from a composite material of silver nanoparticles and elastomeric fibres. *Nat. Nanotechnol.* **2012**, 7, 803-809.

(9) Jung, S.; Kim, J. H.; Kim, J.; Choi, S.; Lee, J.; Park, I.; Hyeon, T.; Kim, D. H., Reverse-micelle-induced porous pressure-sensitive rubber for wearable human-machine interfaces. *Adv. Mater.* **2014**, 26, 4825-4830.

(10) Rogers, J. A.; Someya, T.; Huang, Y. G., Materials and Mechanics for Stretchable Electronics. *Science* **2010**, 327, 1603-1607.

(11) Ahn, J. H.; Je, J. H., Stretchable electronics: materials, architectures and integrations. *J. Phys. D: Appl. Phys.* **2012**, 45, 103001.

(12) Bertolazzi, S.; Brivio, J.; Kis, A., Stretching and Breaking of Ultrathin MoS_2. *ACS Nano* **2011**, 5, 9703-9709.

(13) Feng, W.; Zheng, W.; Gao, F.; Chen, X. S.; Liu, G. B.; Hasan, T.; Cao, W. W; Hu, P. A., Sensitive Electronic-Skin Strain Sensor Array Based on the Patterned Two-Dimensional α-In_2Se_3. *Chem. Mater*. **2016**, 28, 4278-4283.

(14) Late, D. J.; Liu, B.; Luo, J. J.; Yan, A. M.; Matte, H. S.; Grayson, M.; Rao, C. N. R.; Dravid, V. P., GaS and GaSe ultrathin layer transistors. *Adv. Mater.* **2012**, 24, 3549-3554.

(15) Li, L. K; Yu, Y. J.; Ye, G. J.; Ge, Q. Q.; Ou, X. D.; Wu, H.; Feng, D. L.; Chen, X. H.; Zhang, Y. B., Black phosphorus field-effect transistors. *Nat. Nanotechnol*. **2014**, 9, 372-377.

(16) Johari, P.; Shenoy, V. B., Tuning the Electronic Properties of Semiconducting Transition Metal Dichalcogenides by Applying Mechanical Strains. *ACS Nano* **2012**, 6, 5449-5456.

(17) Zhang, J.; Hu, P. A.; Wang, X. N.; Wang, Z. L.; Liu, D. Q.; Yang, B.; Cao, W. W., CVD growth of large area and uniform graphene on tilted copper foil for high performance flexible transparent conductive film. *J. Mater. Chem.* **2012**, 22, 18283-18290.

(18) Wu, H.; Huang, Y. A.; Xu, F.; Duan, Y. Q.; Yin, Z. P., Energy Harvesters for Wearable and Stretchable Electronics: From Flexibility to Stretchability. *Adv. Mater.* **2016**, 28, 9881-9919.

(19) Wu, W. Z.; Wang, L.; Li, Y. L.; Zhang, F.; Lin, L.; Niu, S. M.; Chenet, D.; Zhang, X.; Hao, Y. F.; Heinz, T. F.; Hone, J.; Wang, Z. L., Piezoelectricity of single-atomic-layer MoS_2 for energy conversion and piezotronics. *Nature* **2014**, 514, 470-474.

(20) Yang, Y. C.; Li, X.; Wen, M. R.; Hacopian, E.; Chen, W. B.; Gong, Y. J.; Zhang, J.; Li, B.; Zhou, W.; Ajayan, P. M.; Chen, Q.; Zhu, T.; Lou, J., Brittle Fracture of 2D $MoSe_2$. *Adv. Mater*. **2017**, 29, 1604201.

(21) Blees, M. K.; Barnard, A. W.; Rose, P. A.; Roberts, S. P.; McGill, K. L.; Huang, P. Y.; Ruyack, A. R.; Kevek, J. W.; Kobrin, B.; Muller, D. A.; McEuen, P. L., Graphene kirigami. *Nature* **2015**, 524, 204-207.

(22) Hanakata, P. Z.; Qi, Z. A.; Campbell, D. K.; Park, H. S., Highly stretchable MoS_2 kirigami. *Nanoscale* **2016**, 8, 458-463.

(23) Shyu, T. C.; Damasceno, P. F.; Dodd, P. M.; Lamoureux, A.; Xu, L. Z.; Shlian, M.; Shtein, M.; Glotzer, S. C.; Kotov, N. A., A kirigami approach to engineering elasticity in nanocomposites through patterned defects. *Nat. Mater.* **2015**, 14, 785-789.

(24) Tang, Y. C.; Lin, G. J.; Yang, S.; Yi, Y. K.; Kamien, R. D.; Yin, J., Programmable Kiri-Kirigami Metamaterials. *Adv. Mater.* **2017**, 29, 1604262.

(25) Xu, L. Z.; Shyu, T. C.; Kotov, N. A., Origami and Kirigami Nanocomposites. *ACS Nano* **2017**, 11, 7587-7599.

(26) Wang, Z. H.; Zhang, L.; Duan, S. S.; Jiang, H.; Shen, J. H.; Li, C. Z., Kirigami-patterned highly stretchable conductors from flexible carbon nanotube-embedded polymer films. *J. Mater. Chem. C* **2017**, 5, 8714-8722.

(27) Hua, Z. J.; Zhao, Y.; Dong, S. H.; Yu, P. S.; Liu, Y.; Wei, N.; Zhao, J. H., Large stretchability and failure mechanism of graphene kirigami under tension. *Soft matter* **2017**, 13, 8930-8939.

(28) Song, Z. M.; Wang, X.; Lv, C.; An, Y. H.; Liang, M. B.; Ma, T.; He, D.; Zheng, Y. J.; Huang, S. Q.; Yu, H. Y.; Jiang, H. Q., Kirigami-based stretchable lithium-ion batteries. *Sci. Rep.* **2015**, 5, 10988.

(29) Lamoureux, A.; Lee, K.; Shlian, M.; Forrest, S. R.; Shtein, M., Dynamic kirigami structures for integrated solar tracking. *Nat. Commun.* **2015**, 6, 8092.

(30) Wang, Q. H.; Kalantar-Zadeh, K.; Kis, A.; Coleman, J. N.; Strano, M. S., Electronics and optoelectronics of two-dimensional transition metal dichalcogenides. *Nat. Nanotechnol.* **2012**, 7, 699-712.

(31) Yin, Z. Y.; Li, H.; Li, H.; Jiang, L.; Shi, Y. M.; Sun, Y. H.; Lu, G.; Zhang, Q.; Chen, X. D.; Zhang, H., Single-Layer MoS_2 Phototransistors. *ACS Nano* **2012**, 6, 74-80.

(32) Li, Y. L; Rao, Y.; Mak, K. F.; You, Y. M.; Wang, S. Y.; Dean, C. R.; Heinz, T. F., Probing Symmetry Properties of Few-Layer MoS_2 and h-BN by Optical Second-Harmonic Generation. *Nano Lett.* **2013**, 13, 3329-3333.

(33) Zhao, Y. Y.; Luo, X.; Li, H.; Zhang, J.; Araujo, P. T.; Gan, C. K.; Wu, J.; Zhang, H.; Quek, S. Y.; Dresselhaus, M. S.; Xiong, Q. H.,

Interlayer breathing and shear modes in few-trilayer MoS_2 and WSe_2. *Nano Lett.* **2013**, 13, 1007-1015.
(34) Feng, W.; Zheng, W.; Chen, X. S.; Liu, G. B.; Cao, W. W.; Hu, P. A., Solid-State Reaction Synthesis of a InSe/$CuInSe_2$ Lateral p-n Heterojunction and Application in High Performance Optoelectronic Devices. *Chem. Mater.* **2015**, 27, 983-989.
(35) Feng, W.; Zheng, W.; Cao, W. W.; Hu, P. A., Back Gated Multilayer InSe Transistors with Enhanced Carrier Mobilities via the Suppression of Carrier Scattering from a Dielectric Interface. *Adv. Mater.* **2014**, 26, 6587-6593.
(36) Zheng, W.; Feng, W.; Zhang, X.; Chen, X. S.; Liu, G. B.; Qiu, Y. F.; Hasan, T.; Tan, P. H.; Hu, P. A., Anisotropic Growth of Nonlayered CdS on MoS_2 Monolayer for Functional Vertical Heterostructures. *Adv. Funct. Mater.* **2016**, 26, 2648-2654.
(37) Zheng, W.; Lin, J. H.; Feng, W.; Xiao, K.; Qiu, Y. F.; Chen, X. S.; Liu, G. B.; Cao, W. W.; Pantelides, S. T.; Zhou, W.; Hu, P. A., Patterned Growth of P-Type MoS_2 Atomic Layers Using Sol-Gel as Precursor. *Adv. Funct. Mater.* **2016**, 26, 6371-6379.
(38) Zheng, W.; Qiu, Y. F.; Feng, W.; Chen, J. X.; Yang, H. H.; Wu, S. W.; Jia, D. C.; Zhou, Y.; Hu, P. A., Controlled growth of six-point stars MoS_2 by chemical vapor deposition and its shape evolution mechanism. *Nanotechnology* **2017**, 28, 395601.
(39) Landau L.D.; Lifshitz. E. M., *Theory of Elasticity 3rd English edition. Butterworth-Heinemann*: **1986**; pp 196.
(40) Manzeli, S.; Allain, A.; Ghadimi, A.; Kis, A., Piezoresistivity and Strain-induced Band Gap Tuning in Atomically Thin MoS_2. *Nano Lett.* **2015**, 15, 5330-5335.

Insert Table of Contents artwork here